0.6 ng/dl (normal 0.9–1.8 ng/dl), respectively. These data suggest that the patient had hypothyroidism. The presence of anti-thyroglobulin and anti-thyroid peroxidase antibodies indicated autoimmune thyroiditis, and the patient was treated with levothyroxine.

Unexpectedly, immunological studies showed hypergammaglobulinemia in the patient (Table 1). IgG2 levels were within the normal range, but a percentage of an IgG2 subclass (5.41 %) was lower than that in the normal controls (20–30 %). In addition, the patient tested positive for varicella zoster-specific IgG. Although the patient had recurrent pneumococcal infections, the level of pneumococcus-specific IgG2 was only 0.6 μg/ml (normal >3.0 μg/ml). Lymphocyte subpopulations revealed an extremely high frequency of activated (HLA-DR$^+$) CD3$^+$ T cells and memory (CD45RO$^+$) CD4$^+$ and CD8$^+$ T cells, and an extremely reduced number of CD20$^+$ B cells. An analysis of the T-cell receptor Vβ repertoire revealed a strongly skewed pattern in CD8$^+$ T cells but not in the repertoire of CD4$^+$ T cells (data not shown). Lymphocyte proliferation was impaired in response to phytohemagglutinin, and natural killer cell activity was low. T-cell receptor excision circles (TRECs) were quantified by real time-PCR, as previously described [5]. When measured with the patient's neonatal Guthrie card, the copy number of TRECs was lower than normal, but they were well detectable. However, TRECs were undetectable in this patient at the age of 3 years. The delayed-type hypersensitivity skin test, which uses purified protein from tuberculosis, was negative despite the fact that the patient had been immunized with the bacille Calmette–Guérin vaccine. Furthermore, the patient was positive for various autoantibodies, including anti-thyroglobulin and anti-nuclear antibodies.

Table 1 Immunological studies in the patient

Test	Value	Unit	Normal value
Immunoglobulins			
IgG	1659	mg/dl	929 ± 228
IgA	51	mg/dl	56 ± 18
IgM	188	mg/dl	93 ± 27
IgE	62	IU/ml	0–170
IgG subclasses			
IgG1	1220	mg/dl	390.2–955.2
IgG2	72.9	mg/dl	58.5–292.1
IgG3	52.4	mg/dl	11.4–98.8
IgG4	3.0	mg/dl	1.2–76.7
Lymphocyte subpopulations			
CD3	70.3	%	71.4 ± 5.8
CD4	23.4	%	43.2 ± 11.5
CD8	44.2	%	22.3 ± 6.6
HLA-DR/CD3	76.5	%	<1.0
CD45RO/CD4	74.8	%	21.9 ± 4.4
CD45RO/CD8	39.6	%	14.9 ± 5.6
CD20	0.2	%	12.5 ± 6.7
Lymphoproliferative response to mitogen			
Phytohemagglutinin	7438	cpm	20500–56800
Natural killer cell activity	6	%	18–40
TRECs quantification			
At birth	1.011×10^3	copies/μg DNA	$6.2 \pm 3.2 \times 10^3$
Present	Undetectable		
Autoantibodies			
Anti-thyroglobulin	538	IU/ml	<27.9
Anti-thyroid peroxidase	185	U/ml	<0.29
Anti-nuclear	Positive		Negative
Anti-neutrophil	Positive		Negative

Although the patient showed hypergammaglobulinemia, the presence of humoral and cellular immune defects in addition to various autoimmune features suggested a diagnosis of delayed onset ADA deficiency. Therefore, ADA enzyme activity was assayed by the radiochemical thin-layer chromatography method, as previously described [6, 7]. The levels of adenosine nucleotide (AXP) and deoxyadenosine nucleotides (dAXP) in erythrocytes were determined, as previously described [8]. The patient's ADA activity in mononuclear cells was detectable at 8.6 nmol/min/10^8 cells, but this value is approximately one-tenth of activity found in normal controls (102.6 nmol/min/10^8 cells) (Fig. 2). Consistent with this observation, the patient's ADA level in red blood cells (RBC) was 0 nmol/h/mg (normal 26.4 ± 10.0 nmol/h/mg), and the toxic metabolite dAXP levels in RBC were increased to 9.4 % (normal <1 %). These data indicated that the ADA activity observed in the patient might be mild. The parents' ADA levels in RBC were intermediate between that of the patient's level and that of a normal control (mother

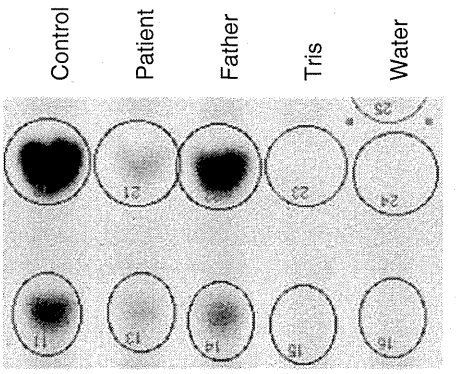

Fig. 2 ADA enzymatic activity. Each lane corresponds to a different sample as follow: control individual (102.6 U), the patient (8.6 U), the patient's father (39.6 U), Tris (1.0 U), and water (1.0 U). U denotes nmol/min/10^8 cells

12.2 nmol/h/mg, father 14.1 nmol/h/mg), which suggests that they are carriers of the ADA deficiency. Gene analysis of *ADA* revealed compound heterozygous mutations in the patient (R156C and V177M), each contributed by one parent: the mother had contributed the R156C mutation and the father passed on a V177M mutation, respectively, thereby confirming the parents' carrier status.

After the diagnosis of delayed onset ADA deficiency, the patient was treated with intravenous immunoglobulin, and he received oral administration of trimethoprim–sulfamethoxazole, and acyclovir. Following the prophylactic treatment, the patient was nearly free from infections. However, serum immunoglobulin levels were decreased (IgG 1069 mg/dl, IgA 21 mg/dl, and IgM 33 mg/dl) at the age of 4 years. Therefore, we searched for a human leukocyte antigen-identical donor and identified his healthy sister as a suitable donor. At the age of 4 years, he underwent a bone marrow transplant preceded by a reduced-intensity conditioning regimen. This regimen included reduced dose intravenous busulfan (8.8 mg/kg total) and fludarabine (total dose: 180 mg/m^2) with standard cyclosporine A prophylaxis. Total nucleated cell and CD34$^+$ cell counts were 6.9×10^8 and 3.1×10^6 cells/kg, respectively. Thus, the patient's condition was good and he exhibited immune reconstitution with nearly complete chimerism.

Discussion

The recurrent infectious episodes in the patient presented herein suggested that he harbored a primary immunodeficiency, and bronchiectasis demonstrated by computed tomography strongly suggested that it was specially a humoral immunodeficiency. Although he had hypergammaglobulinemia, the relatively low frequency of IgG2 subclasses, low levels of pneumococcus-specific IgG2 and the decreased number of B cells demonstrated that the patient had humoral immune defects. Nonetheless, the absolute number of T cells was decreased, and naïve T cells were profoundly diminished in the patient. Impaired lymphocyte proliferation in response to mitogen and the lack of TRECs also indicated that a cellular immune deficiency was present. Hyperproduction of immunoglobulins by scanty B cells suggests that the patient's B cells may be oligoclonal. Furthermore, it remains to be determined whether a specific autoantibody target could be associated with the development of ADEM in this patient, particularly because he also presented with autoimmune disease, such as autoimmune thyroiditis. The combined presence of delayed onset combined immune deficiency and autoimmunity suggested a diagnosis of either delayed onset ADA deficiency or RAG deficiency. Our patient was finally diagnosed with delayed onset ADA deficiency.

The various phenotypes observed in ADA deficiency exhibit a strong correlation with their respective genotypes. For instance, alleles are grouped according to the resulting levels of ADA activity: deletion and nonsense alleles formed Group 0, which assumes no activity, whereas the amino acid substitutions are placed in Groups I–IV with increasing ADA activity [9]. The levels of soluble ADA activity and immunoreactive ADA protein expressed by mutant *ADA* cDNA were measured. ADA proteins bearing the patient's R156C or V177M mutations were included in Groups I and II, respectively. Patients with Group 0 or I alleles might show SCID, whereas patients with Group II might present with delayed onset phenotypes. The phenotype resulting from a combination of R156C and V177M mutations is compatible with that of delayed onset ADA deficiency.

ADEM is defined as a first episode of inflammatory demyelination with polyfocal neurological deficits (altered behavior or consciousness) [4]. MRI features of diffuse, bilateral lesions support ADEM. While the pathophysiology of ADEM remains undefined, it is believed to include autoimmune responses mounted de novo or following an infection. There is no report of an association between ADEM and ADA deficiency, although ADEM is rarely associated with immune deficient individuals. For instance, in one report, a child with common variable immune deficiency was associated with ADEM and Lennox–Gastaut syndrome [10], and ADEM has been observed in several patients with primary HIV infections [11–14]. Abnormal T cells and/or B cells that may be present under conditions of immune deficiency may promote an autoimmune process that results in ADEM. In support of this notion, patients with delayed onset ADA deficiency are frequently associated with autoimmune diseases, including autoimmune thyroiditis. The combination of an oligoclonal T-cell repertoire and a specific autoantibody produced by B cells may contribute to the development of ADEM in the patient. This study suggested that the patient presented ADEM as an autoimmune disease associated with delayed onset ADA deficiency.

Acknowledgments We thank Mr. Hitoshi Moriuchi and Ms. Chikako Sakai for their excellent technical assistance. This work was supported by a Grant-in-Aid for Scientific Research from the Ministry of Education, Culture, Sports, Science and Technology of Japan; and a grant for Research on intractable diseases from the Ministry of Health, Labour, and Welfare of Japan, Tokyo.

References

1. Hershfiled MS. Combined immune deficiency due to purine enzyme defects. In: Stiehm ER, Ochs HD, Winkelstein JA, editors. Immunologic disorders in infants and children. Philadelphia: WB Saunders; 2004. p. 480–504.

2. Hirschhorn R, Candotti F. Immunodeficiency disease due to defects of purine metabolism. In: Ocs HD, Smith CIE, Puck JM, editors. Primary immunodeficiency diseases: a molecular and genetic approach. New York: Oxford University Press; 2007. p. 169–96.
3. Buckley RH, Schiff RI, Schiff SE, et al. Human severe combined immunodeficiency: genetic, phenotypic, and functional diversity in one hundred eight infants. J Pediatr. 1997;130:378–87.
4. Dale RC, Brilot F, Banwell B. Pediatric central nervous system inflammatory demyelination: acute disseminated encephalomyelitis, clinically isolated syndrome, neuromyelitis optica, and multiple sclerosis. Curr Opin Neurol. 2009;22:233–40.
5. Morinishi Y, Imai K, Nakagawa N, et al. Identification of severe combined immunodeficiency by T-cell receptor excision circles quantification using neonatal Guthrie cards. J Pediatr. 2009;155:829–33.
6. Ariga T, Oda N, Yamaguchi K, et al. T-cell lines from 2 patients with adenosine deaminase (ADA) deficiency showed restoration of ADA activity resulted from the reversion of an inherited mutation. Blood. 2001;97:2896–9.
7. Kohn DB, Mitsuya H, Ballow M, et al. Establishment and characterization of adenosine deaminase-deficient human T cell lines. J Immunol. 1989;142:3971–7.
8. Hershfield MS, Buckley RH, Greenberg ML, et al. Treatment of adenosine deaminase deficiency with polyethylene glycol-modified adenosine deaminase. N Engl J Med. 1987;316:589–96.
9. Arredondo-Vega FX, Santisteban I, Daniels S, Toutain S, Hershfield MS. Adenosine deaminase deficiency: genotype-phenotype correlations based expressed activity of 29 mutant alleles. Am J Hum Genet. 1998;63:1049–59.
10. Kondo M, Fukao T, Teramoto T, et al. A common variable immunodeficient patient who developed acute disseminated encephalomyelitis followed by the Lennox-Gastaut syndrome. Pediatr Allergy Immunol. 2005;16:357–60.
11. Allen SH, Malik O, Lipman MCI, Johnson MA, Wilson LA. Acute demyelinating encephalitis (ADEM) in a patient with HIV infection. J Infect. 2002;45:62–4.
12. Morgensen TH, Marinovskij E, Larsen CS. Acute demyelinizating encephalomyelitis (ADEM) as initial presentation of primary HIV infection. Scand J Infect Dis. 2007;39:630–4.
13. Narciso P, Galgani S, Del Grosso B, et al. Acute disseminated encephalomyelitis as manifestation of primary HIV infection. Neurology. 2001;57:1493–6.
14. van Toorn R, Kritzinger F, Rabie H. Acute demyelinating encephalomyelitis (ADEM), cryptococcal reactivation and disseminated Herpes simplex in an HIV infected child following HAART. Eur J Pediatr Neurol. 2005;9:355–9.

Letter to the Editor

Common variable immunodeficiency classification by quantifying T-cell receptor and immunoglobulin κ-deleting recombination excision circles

To the Editor:

Common variable immunodeficiency (CVID) is the most frequent primary immunodeficiency associated with hypogammaglobulinemia and other various clinical manifestations. CVID was originally reported to be a disease primarily caused by defective B-cell function, with defective terminal B-cell differentiation rendering B cells unable to produce immunoglobulin. However, combined immunodeficiency (CID) involving both defective B and T cells is often misdiagnosed as CVID.[1] Indeed, one study reported that $CD4^+$ T-cell numbers were decreased in 29% of 473 patients with CVID[2]; similarly, another study found that naive T-cell numbers were markedly reduced in 44% (11/25) of patients with CVID.[3] These observations indicated that a subgroup of patients with clinically diagnosed CVID is T-cell deficient. Consistently, some patients with CVID have complications that might be related to T-cell deficiency, including opportunistic infections, autoimmune diseases, and malignancies, which is similar to that observed in patients with CID.[1,4] Therefore identifying novel markers to better classify CVID and distinguish CID from CVID will be required to best manage medical treatment for CVID.

We recently performed real-time PCR-based quantification of T-cell receptor excision circles (TREC) and signal joint immunoglobulin κ-deleting recombination excision circles (KREC) for mass screening of severe combined immunodeficiency (SCID)[5] and B-lymphocyte deficiency[6] in neonates. TREC and KREC are associated with T-cell and B-cell neogenesis, respectively.[7] Here we retrospectively report that TREC and KREC are useful for classifying patients with clinically diagnosed CVID.

Hypogammaglobulinemic patients (n = 113) were referred to our hospital for immunodeficiency from 2005-2011, and the following patients were excluded from the CVID pool by estimating their SCID genes based on clinical manifestations and lymphocyte subset analysis: 18 patients with SCID diagnoses; 14 patients less than 2 years of age (transient infantile hypogammaglobulinemia); 10 patients with IgM levels of greater than 100 mg/dL (hyper-IgM syndrome); 26 patients with diseases other than CVID caused by known gene alterations (10 with X-linked agammaglobulinemia and 11 with hyper-IgM syndrome [*CD40L* or *AICDA* mutated]), (2 with DiGeorge syndrome, and 3 with *FOXP3*, *IKBKG*, or *6p* deletions); and 5 patients with drug-induced hypogammaglobulinemia. The remaining 40 patients with decreased IgG (≥2 SDs below the mean for age), IgM, and/or IgA levels, as well as absent isohemagglutinins, poor response to vaccines, or both were included in this study as patients with CVID and analyzed for TREC/KREC levels, retrospectively.

Ages of patients with CVID ranged from 2 to 52 years (median age, 15.5 years). The sex ratio of the patients was 21 male/19 female patients. Serum IgG, IgA, and IgM levels were 370 ± 33 mg/dL (0-716 mg/dL), 30 ± 7 mg/dL (1-196 mg/dL), and 40 ± 6 mg/dL (2-213 mg/dL), respectively. TREC and KREC quantification was performed by using DNA samples extracted from peripheral blood, as reported previously.[5,6] Clinical symptoms were then assessed retrospectively. The study protocol was approved by the National Defense Medical College Institutional Review Board, and written informed consent was obtained from adult patients or parents of minor patients in accordance with the Declaration of Helsinki.

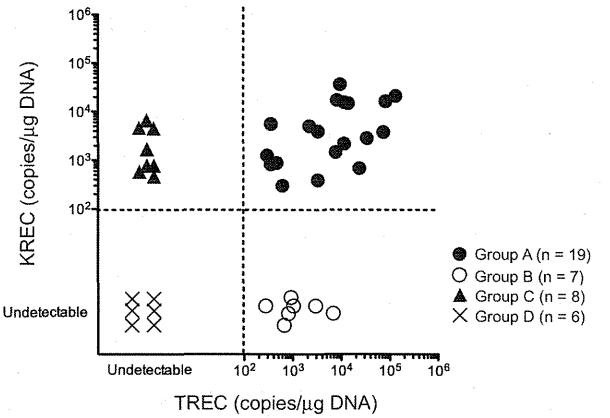

FIG 1. Quantifying TREC and KREC classifies patients with CVID into 4 groups. Patients with CVID were classified as follows: TREC(+)/KREC(+), group A (19 patients); TREC(+)/KREC(−), group B (7 patients); TREC(−)/KREC(+), group C (8 patients); and TREC(−)/KREC(−), group D (6 patients). *Undetectable*, Less than 100 copies/μg DNA.

Based on TREC and KREC copy numbers, the 40 patients with CVID were classified into 4 groups (groups A, B, C, and D; Fig 1). Comparing lymphocyte subsets, $CD3^+$ T-cell numbers were similar among groups A, B, and D but were significantly lower in group C ($P < .05$; group A, 1806 ± 204 cells/μL; group B, 1665 ± 430 cells/μL; group C, 517 ± 124 cells/μL; and group D, 1425 ± 724 cells/μL; $P = .0019$, Tukey multiple comparison test based on 1-way ANOVA). $CD3^+CD4^+CD45RO^+$ memory T-lymphocyte percentages in groups B, C, and D were significantly higher than those in group A ($P < .0001$; group A, 37% ± 16%; group B, 67% ± 13% [$P = .0006$]; group C, 92% ± 8.2% [$P < .0001$]; and group D: 83% ± 14% [$P < .0001$]; see Fig E1 in this article's Online Repository at www.jacionline.org); additionally, the percentages of these cells in groups C and D were higher than in group B ($P = .0115$). These results indicate that group C and D patients have markedly decreased $CD4^+CD45RA^+$ naive T-cell counts than group A patients and that counts in group B are also significantly decreased, although less so than in groups C or D, which is consistent with a report showing lower TREC copy numbers in $CD4^+CD45RO^+$ cells. Some patients in groups B, C, and D exhibited normal $CD4^+CD45RO^+$ percentages, although TREC levels, KREC levels, or both decreased. This discrepancy indicates that TREC/KREC levels could be independent markers to determine the patient's immunologic status in addition to $CD4^+CD45RA^+$; the reasons underlying the discrepancy between $CD4^+CD45RA^+$ and TREC/KREC levels remain unsolved.

$CD19^+$ B-cell numbers in group A were significantly higher ($P < .05$) than those in groups B and D (group A, 269 ± 65 cells/μL; group B, 35 ± 16 cells/μL; group C, 60 ± 11 cells/μL; and group D, 29 ± 16 cells/μL; $P = .0001$). However, B-cell subpopulations, including $CD27^-$, IgD^+CD27^+, and

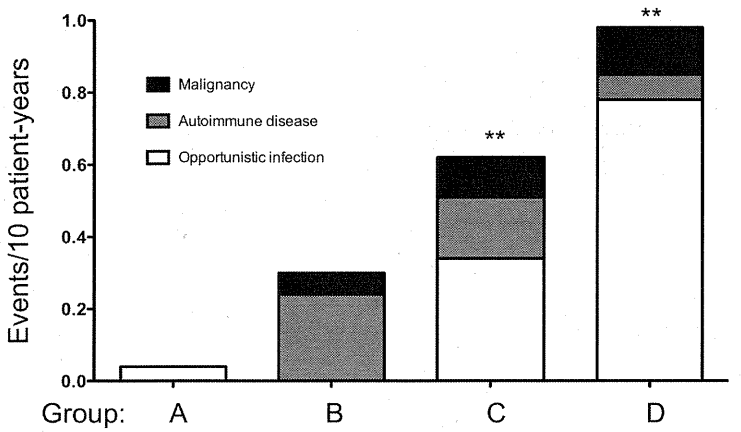

FIG 2. Cumulative incidence of complication events per 10 patient-years differs among groups. Opportunistic infections, autoimmune diseases, and malignancies were evaluated for each patient group. Complication incidences in group D (0.98 events/10 patient-years), group C (0.63 events/10 patient-years), and group B (0.30 events/10 patient-years) were higher than in group A (0.04 events/10 patient-years). Group A versus group D: $^{**}P = .0022$; group A versus C: $^{**}P = .0092$; group A vs group B: $P = .0692$.

IgD^-CD27^+ cells, were not significantly different among the groups. Standardizing KREC copy numbers for each patient by dividing their $CD19^+$ by their $CD27^+$ percentages revealed the same patient classification as that shown in Fig 1 (data not shown), indicating that the original classification was independent of $CD19^+$ B-cell or $CD27^+$ memory B-cell percentages.

Because TREC and KREC levels decrease with age (see Fig E2 in this article's Online Repository at www.jacionline.org)[5,6] and age distribution was wide in this study, we compared patients' ages among groups at the time of analysis to determine whether classification was associated with age. TREC/KREC-based classification was independent of both age and sex because age distribution was not significantly different among groups ($P > .05$; group A, 12.7 ± 2.3 years [2-30 years]; group B, 23.4 ± 4.2 years [6-39 years]; group C, 21.5 ± 6.1 years [4-52 years]; and group D, 25.5 ± 4.4 years [15-46 years]; data not shown) nor was male/female sex ratio (overall, 21/19; group A, 10/9; group B, 2/5; group C, 5/3; and group D, 4/2; $P = .4916$, χ^2 test; data not shown).

We next evaluated whether any correlation existed between TREC/KREC-based classification and clinical symptoms in each patient group. All patients in the study had been treated with intravenous immunoglobulin (IVIG) substitution at the time of analysis. We found that the cumulative events of complications (opportunistic infections, autoimmune diseases, and malignancies) per 10 patient-years were highest in group D (0.98 events/10 patient-years), followed by group C (0.63 events/10 patient-years), group B (0.30 events/10 patient-years), and group A (0.04 events/10 patient-years), where events in groups D and C were significantly higher than group A (group A vs group D, $P = .0022$; group A vs group C, $P = .0092$; group A vs group B, $P = .0692$; Fig 2). Furthermore, we found similar results when evaluating only patients 19 years old or older for group D (1.01 events/10 patient-years), group C (0.56 events/10 patient-years), group B (0.32 events/10 patient-years), and group A (0.06 events/10 patient-years; group A vs group D, $P = .0074$; group A vs group C, $P = .0407$; group A vs group B, $P = .1492$; data not shown). Categorizing patients by using several different previously reported CVID classifications (focused primarily on separating patients based on levels of circulating B-cell subsets), we found that no classification scheme showed any significant event increases in any particular group (see Fig E3 in this article's Online Repository at www.jacionline.org). Assessing longitudinal cumulative opportunistic infection incidence among the groups, group D and C values were significantly higher than in group A (see Fig E4, A, in this article's Online Repository at www.jacionline.org; $P = .0059$). Autoimmune and malignant diseases ($P = .5168$ and $P = .6900$, respectively) were observed in groups B and D but not in group A (see Fig E4, *B* and *C*). Cumulative events were significantly different between groups ($P = .0313$, log-rank test; group A, 5.3% and 5.3%; group B, 14.3% and 57.1%; group C, 27.1% and 63.5%; and group D, 33.3% and 83.3% at 10 and 30 years of age, respectively; see Fig E4, *D*). One patient in group D died of *Pneumocystis jirovecii* pneumonia, and 2 other patients in the same group received hematopoietic stem cell transplantation after complications caused by EBV-related lymphoproliferative disorder.

Assessing these data, TREC/KREC-based classification matches clinical outcomes. Because group D patients exhibited the most frequent complications (opportunistic infections, autoimmune diseases, and malignancies), they could receive a diagnosis of CID based on these symptoms. If they are indeed determined to have CID, then TREC/KREC analysis is helpful to distinguish between CID and CVID. Their TREC(−)/KREC(−) phenotype might relate to defective V(D)J recombination in T- and B-cell development[8] because patients with B-negative SCID (*RAG1*, *RAG2*, *Artemis*, and *LIG4*), as well as patients with ataxia-telangiectasia (AT) and Nijmegen breakage syndrome (NBS; see Fig E5 in this article's Online Repository at www.jacionline.org),[5,6] were also negative for both TREC and KREC; it is intriguing to speculate that an unknown V(D)J recombination gene or genes is responsible. As for treatment, hematopoietic stem cell transplantation should be considered the preferred treatment to "cure" group D patients, as reported in patients with severe CVID/CID, because event-free survival is poor.[9]

In contrast to group D patients, TREC(+)/KREC(+) group A patients treated with IVIG substitution therapy remained healthy. One possible explanation is that these patients harbor

defects only in terminal B-cell differentiation, but not in T cells, and represent typical patients with CVID, as originally reported.

Group C patients had a high frequency of both opportunistic infections and malignancies, suggesting that these TREC(−) patients have T-cell defects. Although group C patients had a similar TREC/KREC pattern to patients with SCID with B cells (*IL2RG* and *JAK3*; see Fig E5, *A*), they do not fulfill the European Society for Immunodeficiencies criteria for SCID, and no mutation was identified in the SCID genes estimated from clinical manifestation and lymphocyte subset analysis. However, from our data, they would likely benefit from undergoing similar treatment to patients with SCID or CID to prevent these complications.

Although opportunistic infections were rare in group B patients, autoimmune diseases were often observed. This is consistent with this group being TREC(+)/KREC(−) and the idea that balance between T and B cells is important to prevent autoimmune diseases in patients with CVID.[1] Intriguingly, a group of patients with AT and NBS were also TREC(+)/KREC(−) (see Fig E4, *B*), which is similar to group B patients. Additionally, $CD45RA^{+}CD4^{+}$ naive T-cell numbers were reduced in most group B patients, which is similar to the phenotype exhibited by patients with AT and NBS. This finding raises the possibility that although some group B patients are also T-cell deficient, as well as B-cell deficient, and should be treated similarly to patients with CID, other patients have only B-cell deficiency and are effectively treated with IVIG substitution therapy.

By analyzing a large CVID patient cohort, the overall survival rate of patients with more than 1 complication was worse than that for patients without other complications.[4] Our findings indicate that low TREC levels, KREC levels, or both are useful markers that correlate well with the overall survival rate in patients with CVID. Therefore we conclude that TREC and KREC are useful markers to assess the clinical severity and pathogenesis of each patient with CVID and to distinguish CID from CVID. Thus patient classification based on TREC/KREC levels would provide a helpful tool for deciding on an effective treatment plan for each patient with CVID.

We thank the following doctors who contributed patient data to this study: Satoshi Okada, Kazuhiro Nakamura, Masao Kobayashi, Tomoyuki Mizukami, Yoshitora Kin, Hironobu Yamaga, Shinsuke Yamada, Kazuhide Suyama, Chihiro Kawakami, Yuko Yoto, Kensuke Oryoji, Ayumu Itoh, Takao Tsuji, Daisuke Imanishi, Yutaka Tomishima, Minako Tomiita, Kaori Sasaki, Akira Ohara, Hanako Jimi, Mayumi Ono, Daisuke Hori, Yuichi Nakamura, Yoshitoshi Otsuka, Toshiyuki Kitoh, Toshio Miyawaki, Akihiko Maeda, Terumasa Nagase, Takahiro Endo, Yoshiaki Shikama, Mikiya Endo, Satoru Kumaki, Lennart Hammarström, Janine Reichenbach, and Reinhard Seger. We also thank Professor Junichi Yata for critical reading and Ms Kaori Tomita, Ms Kimiko Gasa, and Ms Atsuko Kudo for their skillful technical assistance.

Chikako Kamae, MD[a]
Noriko Nakagawa, MD, PhD[a]
Hiroki Sato, MS[b]
Kenichi Honma, MD[a]
Noriko Mitsuiki, MD[c,d]
Osamu Ohara, PhD[c]
Hirokazu Kanegane, MD, PhD[e]
Srdjan Pasic, MD, PhD[f]
Qiang Pan-Hammarström, MD, PhD[g]
Menno C. van Zelm, PhD[h]
Tomohiro Morio, MD, PhD[d]
Kohsuke Imai, MD, PhD[b]
Shigeaki Nonoyama, MD, PhD[a]

From the Departments of [a]Pediatrics and [b]Preventive Medicine and Public Health, National Defense Medical College, Saitama, Japan; [c]the Department of Human Genome Research, Kazusa DNA Research Institute, Chiba, Japan; [d]the Department of Pediatrics, Tokyo Medical and Dental University, Tokyo, Japan; [e]the Department of Pediatrics, University of Toyama, Toyama, Japan; [f]the Department of Immunology, Mother and Child Health Institute, Medical Faculty, University of Belgrade, Belgrade, Serbia; [g]the Department of Laboratory Medicine, Karolinska Institute, Karolinska University Hospital, Huddinge, Stockholm, Sweden; and [h]the Department of Immunology, Erasmus MC, University Medical Center, Rotterdam, The Netherlands. E-mail: kimai.ped@tmd.ac.jp.

Supported in part by grants from the Ministry of Defense; the Ministry of Health, Labour, and Welfare; and the Ministry of Education, Culture, Sports, Science, and Technology.

Disclosure of potential conflict of interest: The authors declare that they have no relevant conflicts of interest.

REFERENCES

1. Yong PFK, Thaventhiran JED, Grimbacher B. "A rose is a rose is a rose," but CVID is not CVID. common variable immune deficiency (CVID), what do we know in 2011? Adv Immunol 2011;111:47-107.
2. Resnick ES, Moshier EL, Godbold JH, Cunningham-Rundles C. Morbidity and mortality in common variable immune deficiency over 4 decades. Blood 2012;119: 1650-7.
3. Moratto D, Gulino AV, Fontana S, Mori L, Pirovano S, Soresina A, et al. Combined decrease of defined B and T cell subsets in a group of common variable immunodeficiency patients. Clin Immunol 2006;121:203-14.
4. Chapel H, Lucas M, Lee M, Bjorkander J, Webster D, Grimbacher B, et al. Common variable immunodeficiency disorders: division into distinct clinical phenotypes. Blood 2008;112:277-86.
5. Morinishi Y, Imai K, Nakagawa N, Sato H, Horiuchi K, Ohtsuka Y, et al. Identification of severe combined immunodeficiency by T-cell receptor excision circles quantification using neonatal Guthrie cards. J Pediatr 2009;155:829-33.
6. Nakagawa N, Imai K, Kanegane H, Sato H, Yamada M, Kondoh K, et al. Quantification of κ-deleting recombination excision circles in Guthrie cards for the identification of early B-cell maturation defects. J Allergy Clin Immunol 2011;128: 223-5.e2.
7. van Zelm MC, Szczepanski T, Van Der Burg M, Van Dongen JJM. Replication history of B lymphocytes reveals homeostatic proliferation and extensive antigen-induced B cell expansion. J Exp Med 2007;204:645-55.
8. Verbsky JW, Baker MW, Grossman WJ, Hintermeyer M, Dasu T, Bonacci B, et al. Newborn screening for severe combined immunodeficiency; the Wisconsin experience (2008-2011). J Clin Immunol 2012;32:82-8.
9. Rizzi M, Neumann C, Fielding AK, Marks R, Goldacker S, Thaventhiran J, et al. Outcome of allogeneic stem cell transplantation in adults with common variable immunodeficiency. J Allergy Clin Immunol 2011;128:1371-2.

http://dx.doi.org/10.1016/j.jaci.2012.10.059

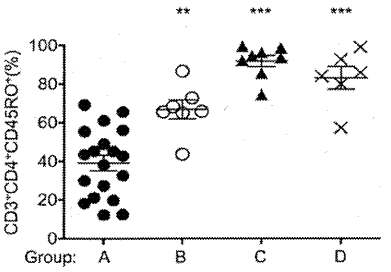

FIG E1. $CD45RO^+CD3^+CD4^+$ T-cell frequency within $CD4^+CD3^+$ lymphocytes was analyzed among groups. $CD45RO^+CD3^+CD4^+$ lymphocyte counts were significantly higher in groups B, C, and D compared with those in group A ($P < .0001$). Group A: 37% ± 16%; group B: 67% ± 13% (**$P < .01$); group C: 92% ± 8.2% (***$P < .001$); and group D: 83% ± 14% (***$P < .001$).

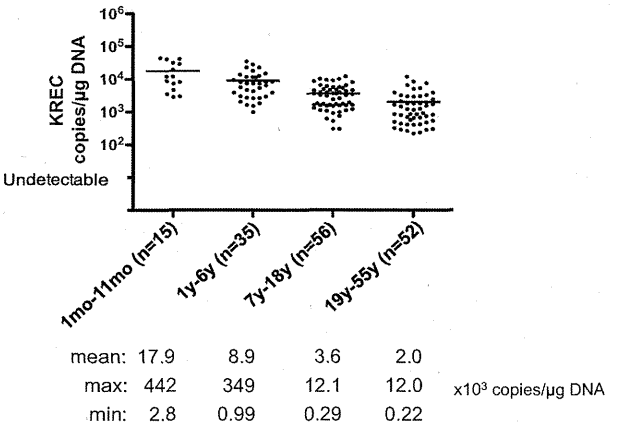

FIG E2. KREC levels were analyzed in genomic DNA samples extracted from peripheral blood of control subjects at different age groups (n = 158; age range, 1 month to 55 years). KREC levels were significantly higher in infants (17.9 ± 3.9 × 10^3 copies/µg DNA) compared with other children's age groups (8.9 ± 1.3 × 10^3 copies/µg DNA in the 1- to 6-year-old group and 3.6 ± 3.8 × 10^3 copies/µg DNA in the 7- to 18-year-old group) and adults (2.0 ± 3.3 × 10^3 copies/µg DNA; $P < .0001$).

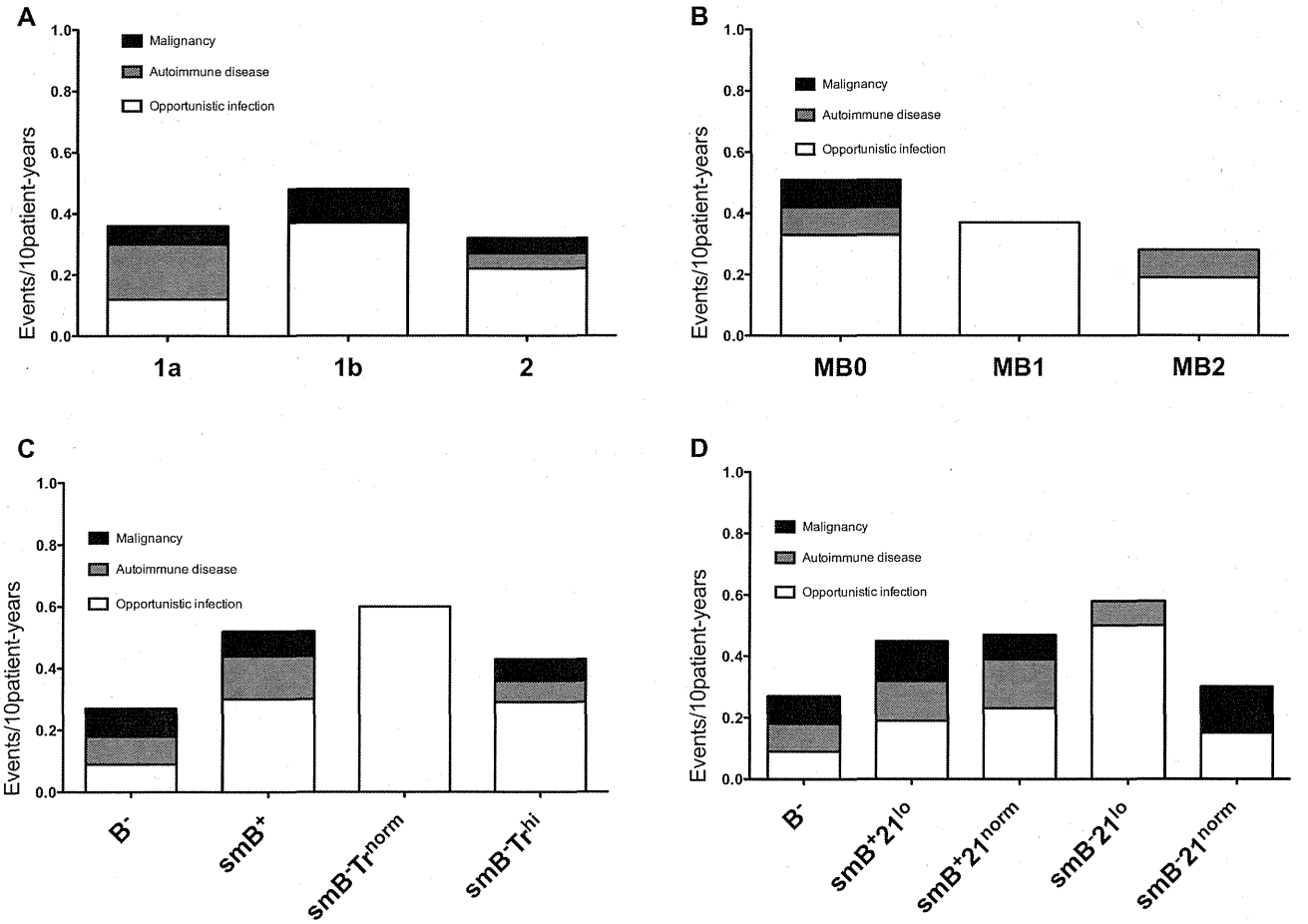

FIG E3. Patients were classified in the following way and analyzed for cumulative incidence of complications: **A,** Freiburg; **B,** Paris; and **C,** EUROclass classifications, according to $CD38^{hi}IgM^{hi}$ transitional B cells (Fig E3, *A-C*) or $CD21^{low}$ B cells **(D)**. Five patients were excluded from the Freiburg and Paris classifications because of decreased B-cell numbers (<1%). Additionally, we excluded 4 patients in the Freiburg classification, 1 patient in the Paris classification, and 4 patients in the EUROclass classification for transitional B cells and 8 in the EUROclass classification for $CD21^{low}$ B cells because of lack of data. The following cumulative events/10 patient-years were found. Freiburg classification: 1a, 0.36; 1b, 0.48; 2, 0.32. Paris classification: MB0, 0.50; MB1, 0.37; MB2, 0.28. EUROclass classification according to transitional B cells: B^-, 0.27; smB^+, 0.52; smB^-Tr^{norm}, 0.60; smB^-Tr^{high}, 0.43. EUROclass classification according to $CD21^{lo}$ B cells: B^-, 0.27; smB^+21^{lo}, 0.45; smB^+21^{norm}, 0.47; smB^-21^{lo}, 0.58; smB^-21^{norm}, 0.30. No classification showed any significantly increased events in any particular group according to calculated *P* values, as follows—Freiburg classification: 1a vs 2 = .898, 1b vs 2 = .479, 1a vs 1b = .838; Paris classification: MB0 vs MB2 = .179, MB1 vs MB2 = .654, MB0 vs MB1 = .764; EUROclass classification according to transitional B cells: B^- vs smB^+ = .298, smB^-Tr^{norm} vs smB^+ = .809, smB^-Tr^{hi} vs smB^+ = .702, smB^-Tr^{hi} vs smB^-Tr^{norm} = .641, smB^-Tr^{norm} vs B^- = .329, smB^-Tr^{hi} vs B^- = .508; EUROclass classification according to $CD21^{lo}$ B cells: B^- vs smB^+21^{norm} = .443, smB^+21^{lo} vs smB^+21^{norm} = .930, smB^-21^{lo} vs smB^+21^{norm} = .695, smB^-21^{norm} vs smB^+21^{norm} = .575, B^- vs smB^-21^{norm} = .926, smB^+21^{lo} vs smB^-21^{norm} = .609, smB^-21^{lo} vs smB^-21^{norm} = .399, B^- vs smB^+21^{lo} = 0.474, B^- vs smB^-21^{lo} = 0.270, smB^+21^{lo} vs smB^-21^{lo} = 0.618.

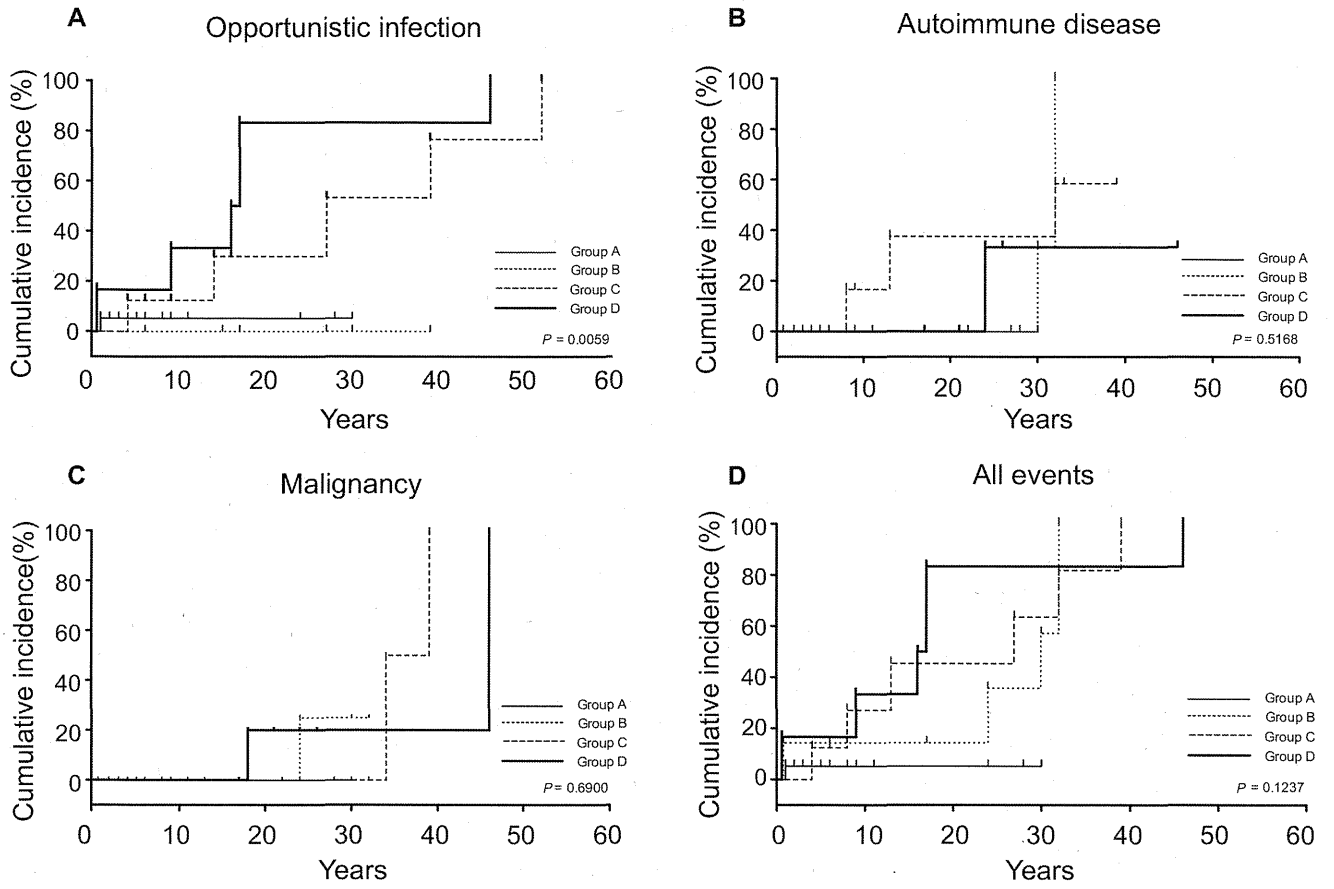

FIG E4. Comparing longitudinal cumulative incidence of complication events among groups. Cumulative incidence was estimated separately and longitudinally by using the Kaplan-Meier method and statistically compared between groups by using the log-rank test. The cumulative incidence of opportunistic infections **(A)**, autoimmune diseases **(B)**, malignancies **(C)**, and all events **(D)** is shown.

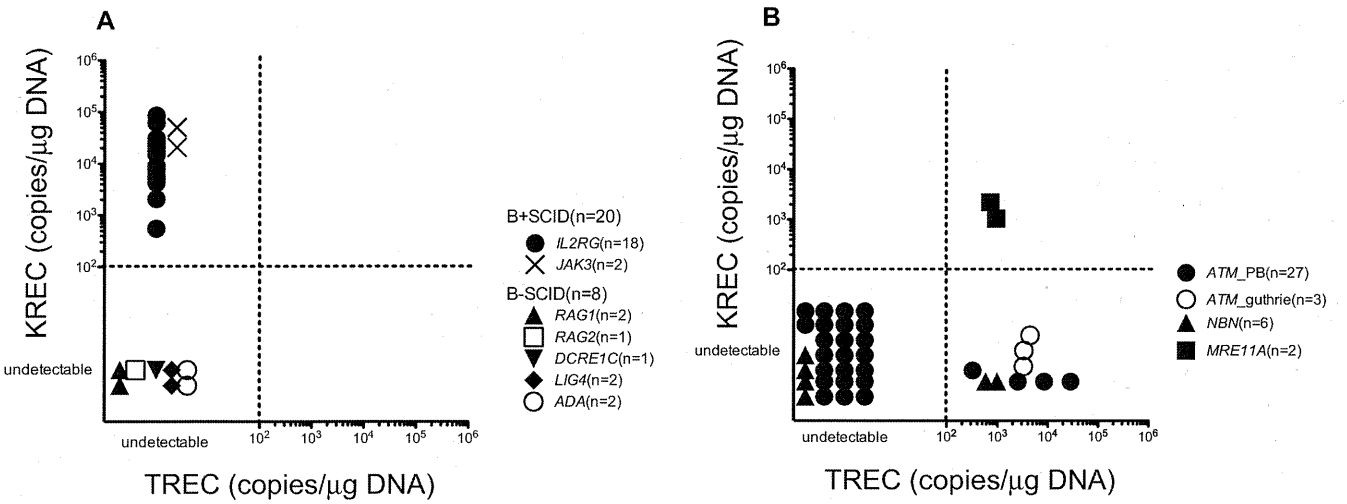

FIG E5. TREC and KREC quantification classifies patients with SCID, AT, NBS, or ataxia-telangiectasia–like disease *(ATLD)* into 4 groups. **A,** Patients with B^+SCID (n = 20) were classified as group C, and patients with B^-SCID (n = 8) were classified as group D; these patients were included in the previous studies.[5,6] **B,** Although most patients with AT (n = 23) and patients with NBS (n = 4) were classified as group D, TRECs were detected in peripheral blood samples (n = 4 in patients with AT and n = 2 in patients with NBS) and neonatal Guthrie cards (n = 3) of some patients with AT, who were classified as group B. Patients with ATLD with *MRE11A* mutations were classified as group A.

blood

2012 120: 1299-1308
Prepublished online June 21, 2012;
doi:10.1182/blood-2012-03-417881

Induced pluripotent stem cells from CINCA syndrome patients as a model for dissecting somatic mosaicism and drug discovery

Takayuki Tanaka, Kazutoshi Takahashi, Mayu Yamane, Shota Tomida, Saori Nakamura, Koichi Oshima, Akira Niwa, Ryuta Nishikomori, Naotomo Kambe, Hideki Hara, Masao Mitsuyama, Nobuhiro Morone, John E. Heuser, Takuya Yamamoto, Akira Watanabe, Aiko Sato-Otsubo, Seishi Ogawa, Isao Asaka, Toshio Heike, Shinya Yamanaka, Tatsutoshi Nakahata and Megumu K. Saito

Blood (print ISSN 0006-4971, online ISSN 1528-0020), is published weekly by the American Society of Hematology, 2021 L St, NW, Suite 900, Washington DC 20036.

Induced pluripotent stem cells from CINCA syndrome patients as a model for dissecting somatic mosaicism and drug discovery

Ta ayu i Tana a [1] a utoshi Ta ahashi [1] Mayu amane [1] Shota Tomida [1] Saori Na amura [1] oichi shima [1] A ira Niwa [1] Ryuta Nishi omori [2] Naotomo ambe [3] Hide i Hara [4] Masao Mitsuyama [4] Nobuhiro Morone [5] ohn . Heuser [5] Ta uya amamoto [1] A ira Watanabe [1] Ai o Sato- tsubo [6] Seishi awa [6] Isao Asa a [1] Toshio Hei e [2] Shinya amana a [1 5 7 8] Tatsutoshi Na ahata [1 2] and Me umu . Saito[1]

[1]Center or iPS Cell Research and Application and [2]Department o Pediatrics yoto University yoto apan [3]Department o Dermatolo y Chiba University raduate School o Medicine Chiba apan [4]Department o Microbiolo y and [5]Institute or Inte rated Cell-Material Sciences yoto University yoto apan [6]Cancer enomics Pro ect University o To yo To yo apan [7] amana a iPS Cell Special Pro ect apan Science and Technolo y A ency awa uchi apan and [8] ladstone Institute o Cardiovascular Disease San Francisco CA

Chronic infantile neurologic cutaneous and articular (CINCA) syndrome is an IL-1–driven autoinflammatory disorder caused mainly by *NLRP3* mutations. The pathogenesis of CINCA syndrome patients who carry *NLRP3* mutations as somatic mosaicism has not been precisely described because of the difficulty in separating individual cells based on the presence or absence of the mutation. Here we report the generation of *NLRP3*-mutant and nonmutant-induced pluripotent stem cell (iPSC) lines from 2 CINCA syndrome patients with somatic mosaicism, and describe their differentiation into macrophages (iPS-MPs). We found that mutant cells are predominantly responsible for the pathogenesis in these mosaic patients because only mutant iPS-MPs showed the disease relevant phenotype of abnormal IL-1β secretion. We also confirmed that the existing anti-inflammatory compounds inhibited the abnormal IL-1β secretion, indicating that mutant iPS-MPs are applicable for drug screening for CINCA syndrome and other NLRP3-related inflammatory conditions. Our results illustrate that patient-derived iPSCs are useful for dissecting somatic mosaicism and that *NLRP3*-mutant iPSCs can provide a valuable platform for drug discovery for multiple NLRP3-related disorders. (*Blood*. 2012;120(6):1299-1308)

Introduction

Chronic infantile neurologic cutaneous and articular syndrome (CINCA syndrome; MIM #607715) is a dominantly inherited autoinflammatory disease characterized by systemic inflammation with an urticaria-like rash, neurologic manifestations, and arthropathy.[1] *NLRP3* mutation is the first and so far the only identified mutation that is responsible for CINCA syndrome.[2,3] *NLRP3* is expressed mainly in myelomonocytic lineage cells and chondrocytes[3] and acts as an intracellular sensor of danger signals from various cellular insults. In normal macrophages, a first stimulus, such as lipopolysaccharide (LPS), induces the synthesis of NLRP3 and the biologically inactive proIL-1β.[4] A second stimulus, such as ATP, enhances the assembly of a protein complex called the NLRP3-inflammasome.[5] The inflammasome contains caspase1, which executes the proteolytic maturation and secretion of IL-1β. Although normal monocytes/macrophages show no or limited IL-1β secretion in response to LPS stimulation alone, CINCA patients' cells exhibit robust IL-1β secretion because the mutant NLRP3-inflammasome is autoactivated without the need for any second stimulus.[6] It is therefore thought that the manifestations of CINCA syndrome are predominantly caused by the excessive secretion of the proinflammatory cytokine, IL-1β, and this concept is supported by the efficacy of an IL-1 receptor antagonist (IL-1Ra) for decreasing most of the symptoms.[7] However, because IL-1Ra treatment does not seem to ameliorate the characteristic arthropathy of cartilage overgrowth and joint contraction,[8] a more specific therapeutic approach that directly modulates the NLRP3-inflammasome is desired.

Although approximately half of CINCA patients carry heterozygous gain-of-function mutations of the *NLRP3* gene,[2,3] 30% to 40% of all patients have mutations in *NLRP3* in only a small number of somatic cells.[9,10] Because the population of mutant cells is relatively small (4.2%-35.8% in blood cells), it remains controversial whether the small fraction of *NLRP3*-mutated cells actually causes the strong autoinflammation observed in CINCA patients, or whether the *NLRP3* mutations found in mosaic patients are just a bystander, with all cells carrying an unknown mutation of another gene that causes the disease.[11]

Somatic mosaicism refers to the presence of more than 1 genetically distinct cell population in a single person, and has been identified in patients with various diseases.[12,13] The relevance of somatic mosaicism to the onset of diseases has been suggested mainly through sequence-based approaches. However, direct evidence that a cell population with a distinct genetic property shows disease-specific characteristics is lacking because it has been impossible to separately extract individual live cells from affected tissues to assess their biologic characteristics. Regarding hematopoietic disorders in which mutant cells show decreased expression of a certain protein, genetic heterogeneity caused by somatic mutations was detected by flow cytometry after intracellular staining,[14-16] but sorting out alive mutant and nonmutant cells for evaluating biologic property has been impossible.

Submitted March 27 2012 accepted May 29 2012. Prepublished online as *Blood* First dition paper une 21 2012 D I 10.1182/blood-2012-03-417881.

The online version o this article contains a data supplement.

The publication costs o this article were de rayed in part by pa e char e payment. There ore and solely to indicate this act this article is hereby mar ed "advertisement in accordance with 18 USC section 1734.

Induced pluripotent stem cells (iPSCs) are pluripotent cell lines directly reprogrammed from somatic cells.[17] Patient-derived iPSCs can provide somatic cells, which cannot be directly obtained from patients, and this discovery has led to the development of a new field of disease modeling (reviewed by Grskovic et al[18]). In addition, iPSC technology has another interesting characteristic that each iPSC clone originates from a single cell,[19] which may make it possible to obtain genetically different iPSC clones from a person.

In this study, we established mutant and nonmutant iPSC lines from the same patients by deriving iPSCs from patients carrying a mutation of an autosomal gene as somatic mosaicism. By analyzing the disease-relevant characteristic of IL-1β secretion, we demonstrated that mutant macrophages are mainly responsible for the disease phenotype in the mosaic patients. Moreover, using a robust differentiation protocol to generate macrophages and purifying them by their surface marker expression, we showed that drug candidates inhibit the IL-1β secretion from mutant macrophages. Our data prove the usefulness of iPSC technology both for dissecting somatic mosaicism and as a platform for drug discovery of multiple NLRP3-related inflammatory diseases.

Methods

Human iPSC generation

We obtained skin biopsy specimens from 2 independent patients (patient 1, CIRA188Ai; and patient 2, CIRA086Ai). This study was approved by Ethics Committee of Kyoto University, and informed consent was obtained from both the patients and their guardians in accordance with the Declaration of Helsinki. We expanded the fibroblasts in DMEM (Nacalai Tesque) containing 10% FBS (Invitrogen) and 0.5% penicillin and streptomycin (Invitrogen). Generation of iPS cells was performed as described previously.[17] In brief, we introduced *OCT3/4*, *SOX2*, *KLF4*, and *c-MYC* using ecotropic retroviral transduction into fibroblasts expressing the mouse *Slc7a1* gene. Six days after transduction, the cells were harvested and replated onto mitotically inactivated SNL feeder cells. The next day, we replaced the medium with Primate ES cell medium (ReproCELL) supplemented with 4 ng/mL bFGF (Wako). Three weeks after this period, individual colonies were isolated and expanded. Cell culture was performed under 37°C, with 5% CO_2 and 21% O_2 unless otherwise stated. Cells were examined using Olympus CKX41 inverted microscope equipped with Nikon Digital Sight DS-L2 camera. A UPlan FLN 4×/0.13 objective (Nikon) was used for image acquisition.

Genetic analysis

Genomic DNA from either fibroblasts or iPSCs was isolated. The PCR product of exon 3 of *NLRP3* was sequenced directly or after subcloning with a TOPO TA cloning kit (Invitrogen), using an ABI 3100 sequencer (Applied Biosystems). For pyrosequencing, the PCR product of exon 3 of *NLRP3* was analyzed by PyroMarkQ96ID (QIAGEN).

RNA isolation and quantitative PCR for *NANOG* and the transgene

Total RNA was purified with the Trizol reagent (Invitrogen) and treated with a Turbo DNA-free kit (Ambion) to remove genomic DNA contamination. A total of 1 μg of total RNA was used for a reverse transcription reaction with ReverTraAce-α (Toyobo) and the dT_{20} primer, according to the manufacturer's instructions. Quantitative PCR was performed on the 7900HT Fast Real-Time PCR System (Applied Biosystems) with SYBR Premix ExTaqII (Takara). The primer sequences are described in supplemental Table 4 (available on the *Blood* Web site; see the Supplemental Materials link at the top of the online article).

Southern blotting

Genomic DNA (5 μg) was digested with BglII and ScaI overnight. The digested DNA fragments were separated on 1% agarose gels and were transferred to a nylon membrane (GE Healthcare). The membrane was incubated with a digoxigenin (DIG)–labeled human *cMYC* DNA probe in DIG Easy Hyb buffer (Roche Diagnostics) at 42°C overnight with constant agitation. After washing, an alkaline phosphatase-conjugated anti-DIG antibody (1:10 000; Roche Diagnostics) was added to a membrane. Signals were obtained using CDP-star (Roche Diagnostics) and detected by an LAS4000 imaging system.

Teratoma formation

Approximately 2×10^6 cells were injected subcutaneously into the dorsal flank of immunocompromised NOD/scid/γc^{null} mice (Central Institute for Experimental Animals). Masses were excised 8 to 10 weeks after injection and fixed with PBS containing 4% paraformaldehyde. Paraffin-embedded tissues were sliced and stained with hematoxylin and eosin. Slides were examined using BIOREVO BZ-9000 (KEYENCE). A PlanApo 20×/0.75 objective (Nikon) and BZ-II Viewer software (KEYENCE) were used for image acquisition.

In vitro differentiation into macrophages

Undifferentiated human embryonic stem cell (ESC) and iPSC lines were cultured on mitotically inactivated SNL feeder cells with Primate ES cell medium supplemented with 4 ng/mL bFGF. During the differentiation of the cells into macrophages, cells were cultured under 37°C, with 5% CO_2 and 5% O_2. On day 0, the iPSCs were plated at a ratio of 1:15 onto a mitotically inactivated OP9 feeder layer on 100-mm cell culture plates in α-MEM (Invitrogen) containing 10% FBS and 1% Antibiotic-Antimycotic (Invitrogen) supplemented with 50 ng/mL VEGFα (R&D Systems). On day 5, the medium was changed. On day 10, the differentiating iPSCs were collected by trypsinization, and Tra-1-85$^+$ CD34$^+$ and KDR$^+$ hematopoietic progenitors were sorted on a FACSAria II instrument (BD Biosciences). The progenitors were plated at 2×10^4 cells on another mitotically inactivated OP9 feeder layer on 100-mm cell culture plates or at 3×10^3 cells/well in 6-well cell culture plates in α-MEM containing 10% FBS and 1% Antibiotic-Antimycotic supplemented with 50 ng/mL IL-3, 50 ng/mL stem cell factor, 10 ng/mL thrombopoietin, 50 ng/mL Flt-3 ligand, and 50 ng/mL M-CSF (all R&D Systems). On day 18, the medium was changed. On day 26, differentiating cells were collected with Accumax (Innovative Cell Technologies), and CD14$^+$ iPSC-derived macrophages were purified on an autoMACSpro instrument (Miltenyi Biotec).

Peripheral blood mononuclear cells (PBs) were obtained from healthy volunteers, and CD14$^+$ monocytes were purified on the autoMACSpro instrument. For macrophage differentiation, 5×10^5 monocytes were plated in 6-well cell culture plates in RPMI 1640 (Sigma-Aldrich) containing 10% FBS and 1% Antibiotic-Antimycotic supplemented with 50 ng/mL M-CSF. On day 5, the adherent cells were collected with Accumax, and CD14$^+$ blood-derived macrophages (B-MPs) were purified on the autoMACSpro instrument. May-Giemsa–stained slides were examined using BIOREVO BZ-9000. A PlanApo 40×/0.95 objective (Nikon) and BZ-II Viewer software were used for image acquisition.

FACS analysis

Hematopoietic marker expression was evaluated on a MACSQuant Analyzer (Miltenyi Biotec). Primary antibodies Tra-1-85-FITC (R&D Systems), CD34-PE (Beckman Coulter), KDR–AlexaFluor-647 (BioLegend), CD45-PE (BD Biosciences PharMingen), and CD14-APC (Beckman Coulter) were used.

Immunocytochemistry

For immunocytochemistry, cells were fixed with PBS containing 4% paraformaldehyde for 5 minutes, permeabilized in PBS containing 0.1% Tween 20 for 5 minutes, and blocked in PBS containing 3% BSA for 10 minutes, all at room temperature. The primary antibody was for CD68 (1:50; Santa Cruz Biotechnology), and the secondary antibody was Cy3-conjugated

AffiniPure Donkey Anti–Mouse IgG (1:100; Jackson ImmunoResearch Laboratories). Nuclei were stained with 1 μg/mL Hoechst 33342 (Invitrogen). Cells were examined using BIOREVO BZ-9000. A Plan Fluor DL 10×/0.30 Ph1 objective (Nikon) and BZ-II Viewer software were used for image acquisition.

Electron microscopy

The 5×10^4 macrophages in 20 μL suspension were placed on the poly-L-lysine treated, carbon-coated sapphire disks (3 mm in diameter) and incubated for 30 minutes at 37°C with 5% CO_2. The cell-adsorbed disk was then subjected to chemical fixation with 2.5% glutaraldehyde in NaHCa buffer (100mM NaCl, 30mM HEPES, 2mM $CaCl_2$, adjusted at pH 7.4 with NaOH). These specimens were postfixed with 1% osmium and 1.5% $K_4Fe(CN)_6$ in 0.1M PBS buffer, washed, dehydrated with a series of ethanol, and embedded in Epoxy resin (TAAB EPON812). After the polymerization at 70°C, the ultra-sections (70 nm) obtained by Ultramicrotome (Leica FC6) were mounted in EM grids, stained with uranyl acetate/lead citrate, and then observed by conventional TEM (JEOL JEM1400).

PCR and microarray analysis of macrophages

Total RNA was column-purified with the RNeasy kit (QIAGEN) and treated with RNase-free DNase (QIAGEN). A total of 20 ng of total RNA was reverse transcribed into cDNA using random primers and the Sensiscript RT Kit (QIAGEN). Quantitative PCR was performed on a StepOne Plus Real-Time PCR System (Applied Biosystems) with TaqMan Gene Expression Master Mix (Applied Biosystems). The primer sequences are described in supplemental Table 4. For the microarray analysis, RNA probes were hybridized to SurePrint G3 Human GE 8 × 60K Microarrays (Agilent Technologies) according to the manufacturer's protocols. Microarrays were scanned, and the data were analyzed using the GeneSpring GX Version 11 software program (Agilent Technologies). The complete dataset from this analysis is available at the NCBI Gene Expression Omnibus using accession no. GSE38626.

LM infection

Listeria monocytogenes EGD (LM) were grown in brain heart infusion broth (Eieken Chemical), washed, suspended in PBS supplemented with 10% glycerol, and stored in aliquots at −80°C. Macrophages were seeded into an 8-well chamber slide at 2×10^5 cells/well in RPMI containing 10% FBS and then infected with bacteria at a multiplicity of infection of 10 for 60 minutes at 37°C. Cells were cultured for further 1 or 5 hours in the presence of 5 μg/mL gentamicin. The cells were fixed in 4% paraformaldehyde and incubated with PBS containing 10% Blocking One (Nacalai Tesque) and 0.1% saponin. F-actin and nuclei were visualized by staining with Alexa-488-phalloidin (Invitrogen) and 4′,6-diamidino-2-phenylindole (Dojindo), respectively. The bacteria were stained by treatment with a goat anti-*Listeria* polyclonal antibody (Kirkegaard & Perry Laboratories) and then with the Alexa 546 anti–goat IgG antibody (Invitrogen). Slides were examined using BIOREVO BZ-9000. A PlanApo_VC 100×H/1.40 objective (Nikon) and BZ-II Viewer software were used for image acquisition, and BZ-II Analyzer (KEYENCE) was used for image processing. Immunofluorescence was evaluated with the IN Cell Analyzer 2000, and samples were analyzed with the IN Cell Developer Toolbox Version 1.8 software program (GE Healthcare).

Cytokine secretion from macrophages

Purified iPS-MPs or B-MPs were seeded at the indicated counts per well or 5×10^4 cells/well unless otherwise stated in 96-well cell culture plates in RPMI 1640 containing 10% FBS and 1% Antibiotic-Antimycotic. Cells were cultured for 2 hours in the presence or absence of inhibitors. The plates were centrifuged at 300*g* for 10 minutes; then the medium was changed. Cells were cultured for 4 hours in the presence of LPS or recombinant human IL-1β. LPS concentration was 1 μg/mL unless otherwise stated. After the 30 minute or 1-hour culture after the addition of 1mM ATP (Sigma-Aldrich), we collected the supernatants and cell lysates. As second signal stimulants, we also used 500 μg/mL silica crystals (U.S. silica) for 1 hour, or 100 μg/mL monosodium urate crystals (Sigma-Aldrich) for 3 hours. For the supernatant transfer experiments, we harvested the supernatant from the wells of mutant or wild-type iPS-MPs, which were stimulated with LPS for 4 hours. After centrifugation, we transferred the supernatants to the wells of other iPS-MPs and cultured them for another 4 hours. The cytokine concentration of the supernatants was determined using a Th1/Th2 11plex FlowCytomix Kit (Bender MedSystems) following the manufacturer's instructions. Reagents were purchased as follows: CA074Me (Calbiochem), IL-1Ra (R&D Systems), oxidized ATP (oATP; Sigma-Aldrich), pyridoxalphosphate-6-azophenyl-2′,4′-disulphonic acid (PPADS; Sigma-Aldrich), cycloheximide (Sigma-Aldrich), MG132 (Calbiochem), Bay11-7082 (Sigma-Aldrich), and Ac-YVAD-CHO (Calbiochem).

LDH secretion assay

The lactate dehydrogenase (LDH) concentration of the supernatants of iPS-MPs after a 4-hour culture with LPS was determined with an LDH Cytotoxicity Detection kit (Takara) following the manufacturer's instructions.

Statistical analysis

The data were processed using the SPSS Statistics Version 18 software package. The values are reported as the mean ± SEM. Comparisons between groups were performed using the unpaired Student *t* test. $P < .05$ was considered statistically significant.

Results

Establishment and characterization of iPSCs

Dermal fibroblasts were obtained from 2 male CINCA patients who had mutations of *NLRP3* as somatic mosaicism. Both patients had nonsynonymous point mutations in the *NLRP3* coding region. The fibroblasts from patients 1 and 2 contained 34% and 9.8% mutant cells, respectively (Figure 1A; supplemental Figure 1A). These fibroblasts were reprogrammed to iPSCs after transduction with retroviral vectors encoding *OCT3/4*, *SOX2*, *KLF4*, and cMYC.[17] Twelve of the 28 isolated clones from patient 1, and 3 of 30 clones from patient 2 had a heterozygous mutation of the *NLRP3* gene, whereas the rest of the clones were wild-type (Figure 1A; supplemental Figure 1B-C). The frequency of mutants was comparable among blood cells,[9,20] fibroblasts, and iPSCs (Table 1). We randomly selected 3 mutant (M1-M3) and 3 wild-type clones (W1-W3) from patient 1 and 3 mutant (m1-m3) and 3 wild-type clones (w1-w3) from patient 2 for the propagation and subsequent analyses.

All iPSC clones showed a characteristic human ESC-like morphology (Figure 1B), the reactivation of endogenous pluripotency genes (*OCT3/4*, *SOX2*, *NANOG*; Figure 1C-D; supplemental Figure 1D) and the demethylation of the *OCT3/4* promoter regions (supplemental Figure 1E). Transgene expression was rarely detected (Figure 1D; supplemental Figure 1D), and the retroviral integration patterns were confirmed by a Southern blot analysis (Figure 1E; supplemental Figure 1F). All of the iPSC clones maintained a normal karyotype (data not shown). There were neither proviral integration nor copy number changes observed in any of the genes that might affect the function of the NLRP3 inflammasome (supplemental Tables 1 and 2). Genetic identity was proven by a short tandem repeat analysis (supplemental Table 3), and the pluripotency of the iPSC clones was confirmed by the presence of cell derivatives of all 3 germ layers by teratoma formation after injection of undifferentiated iPSCs into immunocompromised NOD/scid/γc^{null} mice (Figure 1F; supplemental Figure 1G).

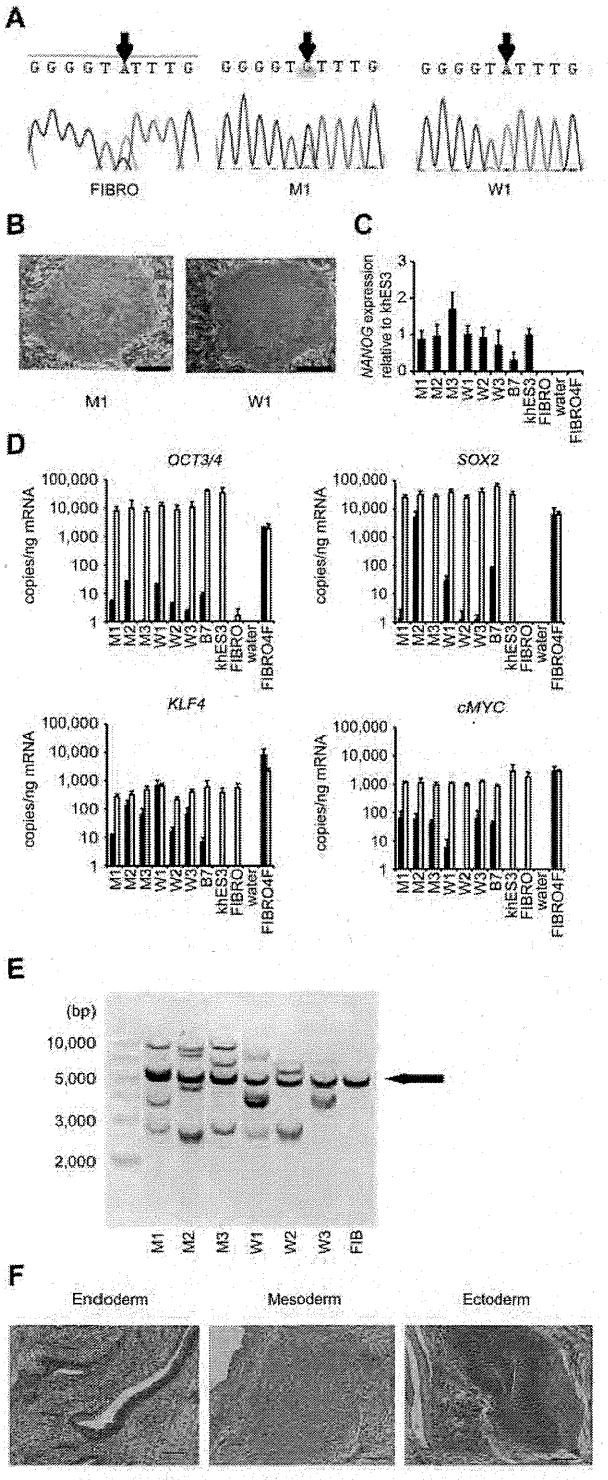

Figure 1. Establishment and characterization of iPSCs. (A) Se uencin o the *NLRP3* 1709 A > mutation (570C) in broblasts (FIBR) mutant iPSCs (M1) and wild-type iPSCs (W1) in patient 1. (B) The morpholo y o the mutant and wild-type iPSCs. (C) *NANOG* e pression in CINCA iPSCs control iPSCs (B7) control SCs (h S3) broblasts (FIBR) and broblasts transduced with 4 actors (FIBR 4F) normali ed to *GAPDH*. n = 3. (D) A uantitative RT-PCR assay or the e pression o *OCT3/4 SOX2 KLF4* and *cMYC* in iPSCs. ne primer set detects only the trans ene (in blac) and the other primer set detects both the trans ene and endo enous ene (in white). n = 3. ( ) Retroviral trans ene inte ration analyses. Southern blot analyses were per ormed with DI -labeled DNA probes a ainst *c-MYC*. The parental broblasts carried a band in common with all o the iPSC lines (arrow). (F) A teratoma derived rom a mutant iPSC clone M1. Scale bars represent 100 μm. Data are mean ± S M.

Differentiation and characterization of iPSC-derived macrophages

To compare the most prominent features of the disease, we differentiated the patient-derived iPSCs into the monocyte/macrophage lineage using a murine stromal cell line, OP9.[21] After culturing the iPSCs on an OP9 feeder layer for 10 days, we collected KDR$^+$ CD34$^+$ hemangioblasts (Figure 2A). All of the iPSC clones, whether they carried an *NLRP3* mutation or not, differentiated into KDR$^+$ CD34$^+$ progenitors as efficiently as the control ESC or iPSC clones (Figure 2B; supplemental Figure 2A). Adherent CD68$^+$ macrophages emerged after culturing the KDR$^+$ CD34$^+$ cells on another OP9 feeder layer for 16 days (Figure 2C; supplemental Figure 2B). Approximately 80% of the differentiated cells expressed CD14, and magnetic-activated cell sorting increased the purity to almost 100% (Figure 2D). All of the clones we used efficiently produced comparable amounts of iPSC-derived macrophages (iPS-MPs; Figure 2E; supplemental Figure 2C). The iPS-MPs visualized by light and electron microscopy showed a typical morphology, with a high cytoplasm-to-nucleus ratio and cytoplasmic vacuoles (Figure 2F; supplemental Figure 2D). The iPS-MPs showed a global gene expression pattern closer to that of blood-derived macrophages than to the parental iPSC clone (supplemental Figure 2E-F). Both mutant and wild-type iPS-MPs phagocytosed bacteria to the same extent when we infected the cells with Gram-positive LM, an intracellular bacterium that escapes into the cytosol (Figure 2G-H). These data indicate that both the mutant and wild-type iPS-MPs derived from mosaic CINCA patients are indistinguishable based on their gene expression and their phagocytic function.

Elucidation of the pathogenesis of somatic mosaic CINCA syndrome

Monocytes derived from CINCA syndrome patients usually do not spontaneously secrete IL-1β and become active after LPS stimulation.[6] Monocytes or mononuclear cells from untreated CINCA syndrome patients, however, sometimes show an increased synthesis of proIL-1β[2] and secretion of mature IL-1β,[7] even in the absence of LPS stimulation, because they can be activated by persistent inflammation or by the purification procedure. As spontaneous activation complicates the functional analysis, we herein evaluated the IL-1β activation status both before and after the stimulation. We observed that the mRNA expression of *IL1B* was low in unstimulated iPS-MPs and increased to comparable levels in mutant and wild-type iPS-MPs in response to LPS stimulation (supplemental Figure 3A). Similarly, the mRNA level of *NLRP3* was relatively low before LPS stimulation (supplemental Figure 3A). Mature IL-1β was not detectable in the supernatant of the cell culture medium (data not shown). Collectively, these data indicate that the unstimulated iPS-MPs were in an "inactive" state before stimulation.

To identify which iPS-MP clones showed the specific features compatible to patients' monocytes, we evaluated their IL-1β secretion. Although LPS stimulation alone led to IL-1β secretion

Table 1. Mutation frequency among different cell types

		Frequency (%) of mutant cells		
Patient no.	Site of mutation	Whole blood	Fibroblasts	iPSCs
1	1709A > (570C)	33.3	34.3	42.9
2	919 > A(307S)	8.5	9.8	10.0

The re uency in whole blood was reported previously.[9 20]

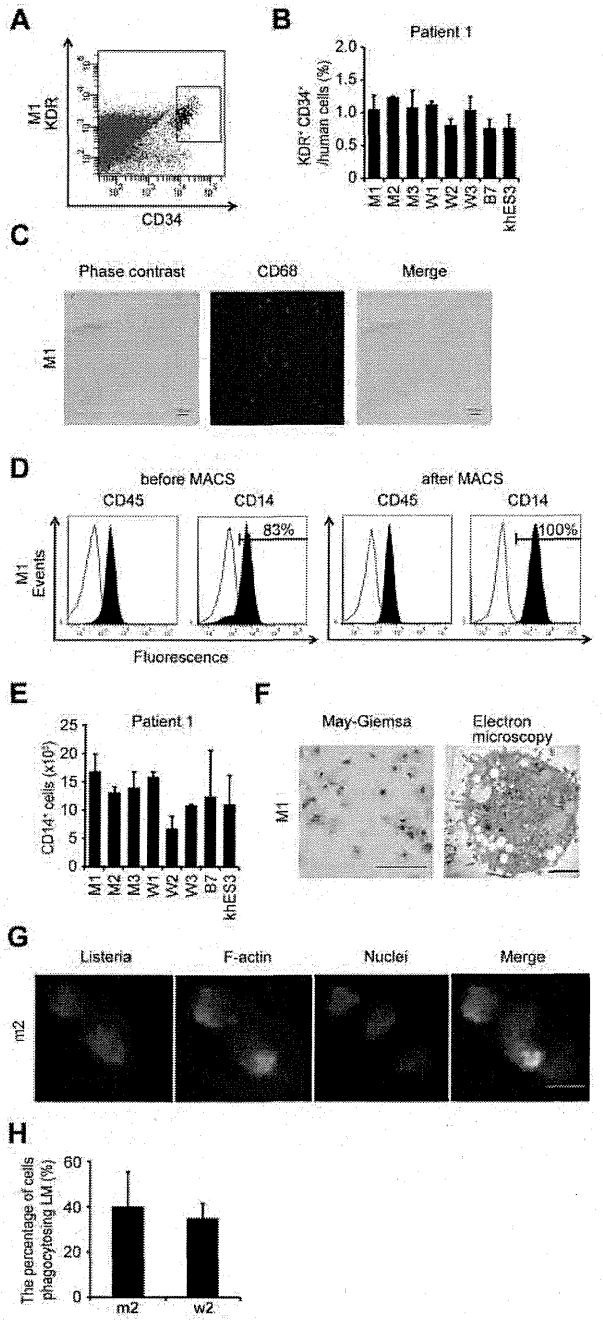

Figure 2. Differentiation and characterization of iPSCs-derived macrophages. (A) DR+ CD34+ hematopoietic pro enitors puri ed 10 days a ter di erentiation. (B) The percenta e o DR+ CD34+ cells in Tra-1-85+ human cells. n = 3. (C) CD68 immunostainin o macropha es. Scale bars represent 100 μm. (D) The histo rams show antibody stainin (in blac) relative to the isotype-matched controls (in white) or a blood cell mar er (CD45) and a macropha e mar er (CD14) in cells be ore (le t 2 panels) or a ter (ri ht 2 panels) ma netic-activated cell sortin puri cation. ( ) CD14+ cell counts obtained rom iPSCs plated on an P9 eeder layer on one 100-mm dish. n = 3. (F) Representative morpholo y o iPS-MPs evaluated by May- iemsa stainin or transmission electron microscopy. Scale bars represent 100 μm and 2 μm respectively. ( ) The pha ocytosis by iPS-MPs a ter LM in ection. The cells were treated with anti-LM antibody phalloidin and 4′ 6-diamidino-2-phenylindole. Scale bar represents 20 μm. (H) The percenta e o iPS-MPs pha ocytosin LM was calculated as the avera e o 9 elds o vision. Data are mean ± S M.

from the mutant iPS-MPs, the addition of ATP was necessary to induce IL-1β secretion from wild-type iPS-MPs, as it was from either ESC-derived or blood-derived macrophages (Figure 3A). The IL-1β level from mutant iPS-MPs was significantly higher than that from wild-type macrophages, even in the presence of LPS plus ATP. Both groups of macrophages showed similar kinetics in their secretion of other cytokines, such as IL-6 or TNFα (Figure 3A). The results were similar in the iPS-MPs from patient 2 (Figure 3B). Although iPS-MPs showed a similar response at lower LPS concentrations (Figure 3C-D; supplemental Figure 3B-C), no IL-1β secretion was detectable from mutant iPSCs, wild-type iPSCs, or parental fibroblasts in response to stimulation with 1 μg/mL LPS (data not shown). These data demonstrate that the abnormal function of the iPS-MPs is predominantly determined by the *NLRP3* mutation, and not by some unknown genetic alteration(s) prevalent in all cells. We next investigated whether iPS-MPs show pyronecrosis: a pathogen-induced, cathepsin B-dependent, necrosis-like programmed cell death that is characteristically observed in *NLRP3*-mutant monocytes/macrophages.[22,23] When we compared LDH secretion as a marker of membrane rupture, we found that LPS stimulation evoked a significantly higher LDH secretion only from the mutant iPS-MPs, which was inhibited by the cathepsin B inhibitor, CA074Me (Figure 3E).

Despite the low percentage of mutant cells, the clinical manifestation of mosaic CINCA patients is similar to that of patients with a heterozygous mutation.[9,10] We hypothesized that an interaction between the mutant and wild-type macrophages leads to exacerbation of the inflammation. To test this hypothesis, we modeled a mosaic condition by coculturing mutant and wild-type cells. After stimulating mutant iPS-MPs with LPS in separate cultures or in cocultures with wild-type counterparts, we determined the IL-1β level in the supernatant. We found that the IL-1β secretion significantly increased after coculture (Figure 4A; supplemental Figure 4A). Although increasing the cell concentration raised the total amount of the IL-1β secretion from mutants, it did not accelerate the IL-1β secretion per cell from mutant iPS-MPs or enhance the secretion from wild-type macrophages (Figure 4B). To determine the ratio of mutant/wild-type cells at which the additional IL-1β secretion is most enhanced, we changed the ratio using a fixed number of mutant iPS-MPs and increasing the number of wild-type iPS-MPs. We observed a significant increase only at a percentage of 25% mutant macrophages (Figure 4C). Thus, we capitulated, at least in part, the patient's mosaic condition in vitro.

Next, we tried to elucidate whether the interaction is mediated by some humoral factor(s), but supernatant transfer did not facilitate the IL-1β secretion (Figure 4D). As a candidate that may mediate this interaction, we selected ATP because necrotic cells trigger NLRP3-inflammasome activation in part through ATP release.[24] We therefore investigated whether the necrosis-induced ATP secretion activates the wild-type iPS-MPs using ATP receptor antagonists, oxidized ATP (oATP) and PPADS. Although both antagonists markedly inhibited the IL-1β secretion after LPS plus ATP stimulation (supplemental Figure 4B), neither of them abrogated the additional IL-1β secretion in the mixed culture (Figure 4E; compare column 2 with column 3, and column 4 with column 5). The IL-1β secretion from mutant iPS-MPs may have decreased because of off-target effects of oATP.[25] Overall, although it remains to be elucidated how this effect is mediated, these results suggest that the interaction between mutant and wild-type macrophages may enhance IL-1β secretion in mosaic patients.

Validation for future applications for drug screening

An NLRP3-targeted therapeutic approach would be attractive because (1) the progressive arthropathy despite anti–IL-1 therapy indicates that the presence of additional proteins processed by the

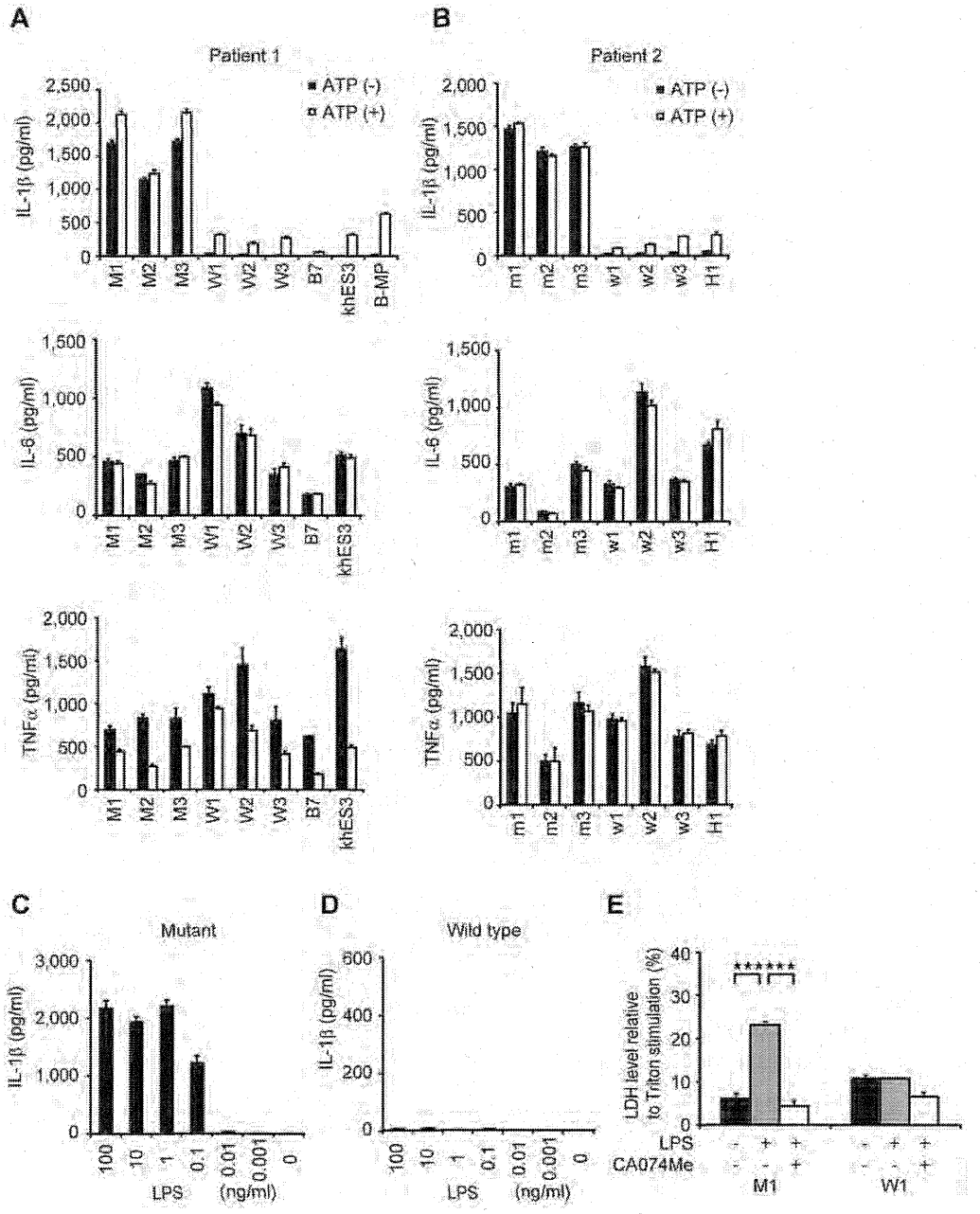

Figure 3. Elucidation of the pathogenesis of somatic mosaic CINCA syndrome. (A) Cyto ine secretion rom iPS-MPs derived rom patient 1. A ter stimulatin iPS-MPs by LPS with or without ATP we determined the IL-1β (top panel) IL-6 (middle panel) or TNFα (bottom panel) level o the supernatant. n = 3. (B) Cyto ine secretion rom iPS-MPs derived rom patient 2 determined as in panel A. (C) IL-1β secretion rom mutant iPS-MPs in the presence o 10- old dilutions o LPS rom 100 n /mL. n = 3. (D) IL-1β secretion rom wild-type iPS-MPs determined as in panel C. ( ) LDH secretion rom iPS-MPs stimulated with LPS in the presence or absence o the cathepsin B inhibitor CA074Me. n = 3. Data are mean ± S M. $P < .001$ (Student t test).

inflammasome is also involved in the pathogenesis of CINCA syndrome; (2) specific inhibition of the NLRP3-inflammasome can avoid unfavorable suppression of other IL-1β–processing pathways in response to various triggers; and (3) these drugs may be also effective for various other NLRP3-related chronic inflammatory conditions, such as Alzheimer disease, diabetes, severe gout, and atherosclerosis.[26-30] Because drug screening using NLRP3 autoactivated cells has not been described previously, we examined whether the iPS-MPs from CINCA patients can serve as a prototype for seeking drug candidates that directly modulate NLRP3-inflammasome activation.

When wild-type iPS-MPs were stimulated with LPS and ATP in the presence of various inhibitors, inhibitors known to modulate molecules upstream of the NLRP3-inflammasome (a protein synthesis inhibitor, cycloheximide, and an NF-κB inhibitor, MG132), downstream of the inflammasome (a caspase-1 inhibitor, Ac-YVAD-CHO), and both upstream of and the inflammasome itself[31] (Bay11-7082) successfully inhibited IL-1β secretion (Figure 5A). Although the precise mechanism is unknown, a cathepsin B inhibitor, CA074Me, also efficiently inhibited IL-1β secretion. As expected, upstream inhibitors inhibited the secretion of other cytokines, such as IL-6 and IL-8, but a downstream inhibitor,

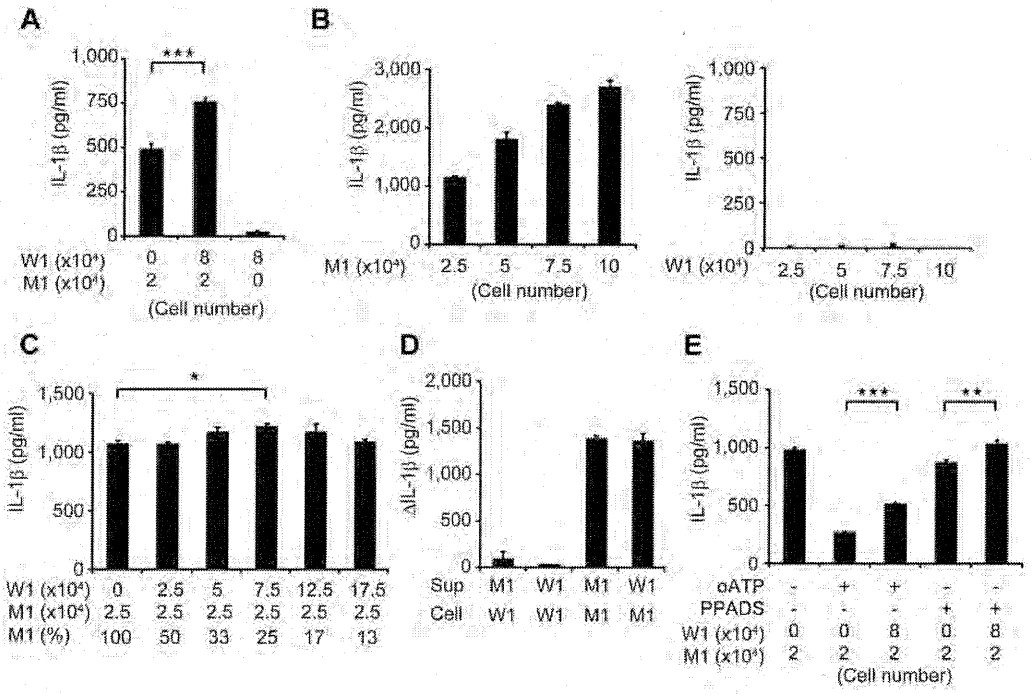

Figure 4. Remodeling mosaicism by coculturing mutant and wild-type iPS-MPs. (A) IL-1β secretion rom cocultured iPS-MPs. We used 2 × 10^4 mutant iPS-MPs (M1) and 8 × 10^4 wild-type iPS-MPs (W1) as indicated. n = 6. (B) IL-1β secretion rom various numbers o mutant (le t panel) or wild-type (ri ht panel) iPS-MPs. The iPS-MPs were seeded at the indicated numbers. n = 3. (C) IL-1β secretion rom iPS-MPs that were cocultured at various ratios. The wild-type or mutant iPS-MPs were seeded at the numbers indicated in the rst and second rows respectively. The percenta e o mutants is indicated in the third row. n = 3. (D) Increase o IL-1β levels durin stimulation by the supernatant. The supernatant was harvested rom the wells o the indicated iPS-MPs (Sup) and trans erred to the wells o other iPS-MPs (Cell) n = 3. ( ) IL-1β secretion rom cocultured iPS-MPs in the presence o the ATP receptor anta onist oATP (300μM) or PPADS (300μM). We used 2 × 10^4 mutant iPS-MPs (M1) and 8 × 10^4 wild-type iPS-MPs (W1) as indicated. n = 6. Data are mean ± S M. $P < .001$ (Student *t* test). $P < .01$ (Student *t* test). $P < .05$ (Student *t* test).

Ac-YVAD-CHO, specifically affected IL-1β secretion (Figure 5A). Although CA074Me and Ac-YVAD-CHO inhibited IL-1β secretion regardless of the second signals that were present, PPADS, an inhibitor of extracellular ATP signaling, failed to inhibit IL-1β secretion by following exposure to other second signals, such as monosodium urate and silica crystals (Figure 5B), proving that wild-type iPS-MPs can be activated in a second signal-dependent manner. Therefore, the results of the wild-type iPS-MP-based compound screening depended on the choice of second signals, and such a screening makes it possible to extract candidate compounds that modulate specific second signaling pathways.

Next, we examined the response of mutant iPS-MPs to the inhibitors. In the absence of inhibitors, mutant iPS-MPs secreted a higher level of IL-1β, but treatment with inhibitors dose-dependently decreased IL-1β secretion to the comparable level produced by WT iPS-MPs (Figure 5C). We thus demonstrated the efficacy of these chemical compounds, even for excessive IL-1β production by constitutively hyperactivated inflammasomes. As expected, the mutant iPS-MPs did not respond to PPADS, confirming their autoactivation in a second signal-independent manner (Figure 5D). Therefore, because they can be activated independently from the type of second signals, mutant iPS-MP–based screening would enable the exclusion of compounds that inhibit IL-1β secretion depending on a specific type of second signal transduction. Overall, through using the IL-1β inhibition as the initial criteria and weeding out upstream inhibitors by measuring the levels of other cytokines, we can use *NLRP3*-mutant iPS-MPs to screen for drugs for CINCA syndrome and possibly for other NLRP3-related chronic inflammatory conditions.

Discussion

Since the first identification of a CINCA syndrome patient carrying *NLRP3* mutation as somatic mosaicism,[20] it has been controversial whether the small fraction of *NLRP3*-mutated cells actually causes the strong autoinflammation. It remained unanswered because of the difficulty to separately obtain live mutant and nonmutant blood cells. In this study, we reprogrammed fibroblasts from mosaic patients and obtained macrophages with different genotypes. By showing that only *NLRP3*-mutant iPS-MPs exhibit the distinct proinflammatory phenotype, we demonstrated that the *NLRP3*-mutant macrophages are mainly responsible for the pathogenesis of mosaic CINCA syndrome.

In this study, we established both *NLRP3*-mutant and nonmutant iPSC clones from the same person. One of the potential limitations of studies with patient-derived iPSCs is the difficulty in obtaining isogenic control counterparts, which do not carry the responsible mutations. One possible strategy to solve this problem is to correct the affected gene locus of patient-derived iPSC clones using novel techniques that facilitate homologous recombination.[32,33] As another solution, both affected and control iPSC clones can be obtained from patients of some X-linked hereditary diseases because each iPSC clone originated from somatic cells carrying either a mutated or nonmutated allele as an active X chromosome.[34-36] In the present study, we have retrieved both mutant and wild-type iPSC clones from patients with somatic autosomal mutations. These clones theoretically have the same genetic backgrounds, except for the *NLRP3* gene, and should serve as an ideal pair of mutant and control clones for disease research.

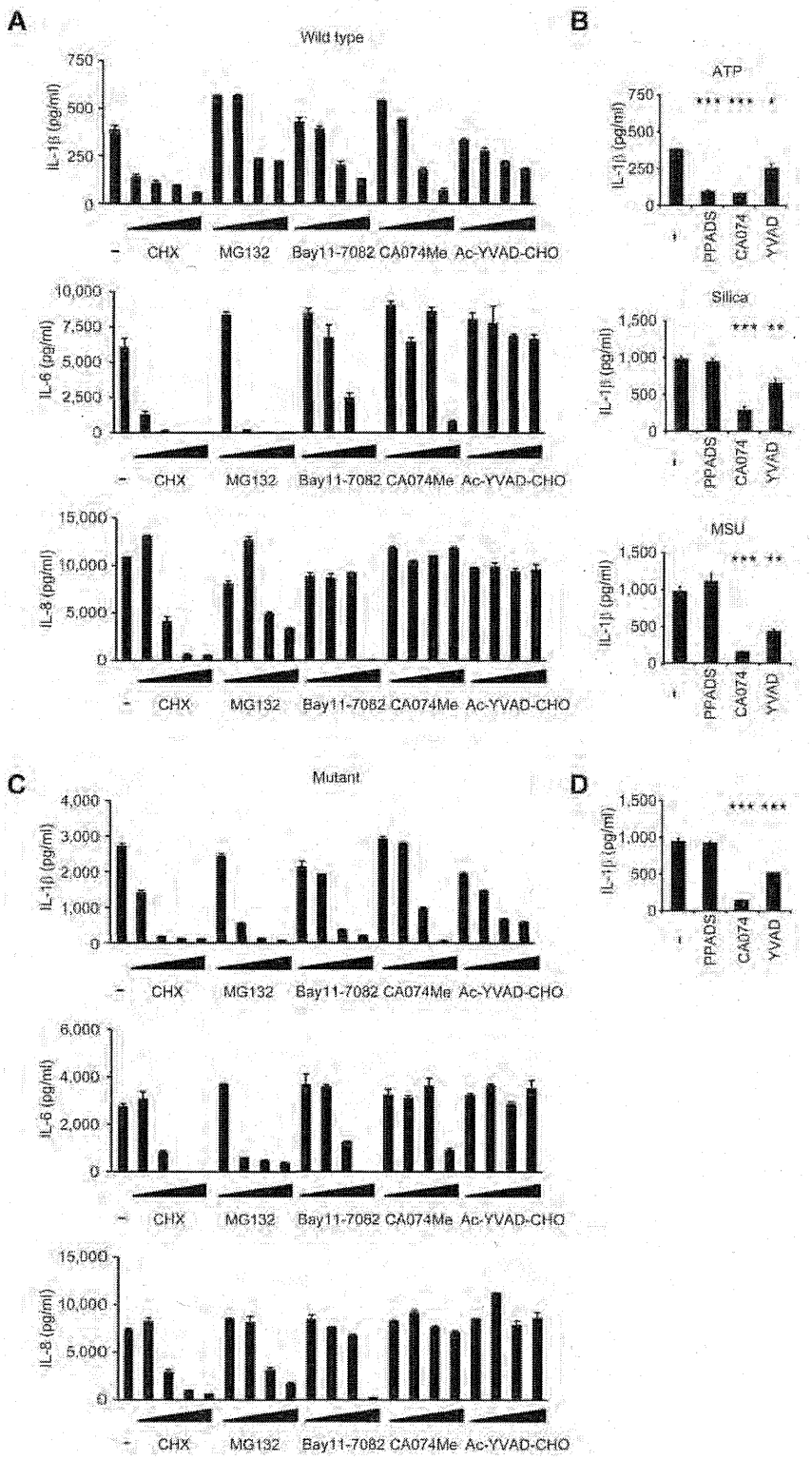

Figure 5. Validation of the cells for future applications for drug screening. (A) Inhibition o IL-1β (top panel) IL-6 (middle panel) or IL-8 (bottom panel) secretion rom wild-type iPS-MPs by various inhibitors. The iPS-MPs were cultured or 2 hours in the presence o 100μM cyclohe imide (CH) 100μM M 132 10μM Bay11-7082 25μM CA074Me 50μM Ac- VAD-CH as well as 10- old dilutions o each inhibitor e cept CA074Me (which was diluted 5- old) ollowed by LPS treatment plus ATP stimulation. n = 3. (B) The di erential inhibition o IL-1β secretion rom wild-type iPS-MPs by various inhibitors. In the presence o inhibitors such as PPADS (300μM) CA074Me (25μM) or Ac- VAD-CH (50μM) LPS-primed wild-type iPS-MPs were stimulated with second si nal tri ers such as ATP or 1 hour (top panel) silica crystals or 1 hour (middle panel) or monosodium urate crystals or 3 hours (bottom panel). n = 3. (C) Inhibition o IL-1β (top panel) IL-6 (middle panel) or IL-8 (bottom panel) secretion rom mutant iPS-MPs by various inhibitors was evaluated as in panel A n = 3. (D) Inhibition o IL-1β secretion rom mutant iPS-MPs by various inhibitors. In the presence o inhibitors such as PPADS (300μM) CA074Me (25μM) or Ac- VAD-CH (50μM) mutant iPS-MPs were stimulated with LPS or 4 hours. n = 3. Data are mean ± S M. $P < .001$ (Student t test). $P < .01$ (Student t test). $P < .05$ (Student t test).

In addition to obtaining isogenic controls, iPSCs from patients with somatic autosomal mutations enable dissection and modeling of somatic mosaicism. Despite the fact that each person contains various minor somatic mutations,[37] the effects of mosaicism can often be overlooked because of the difficulty in assessing the possible biologic effects caused by the small cell populations carrying the genetic alterations. Here we dissected somatic mosaicism by obtaining the component cells with heterogeneous genetic identity separately and established an in vitro model to evaluate the interaction between these cells, although precise mechanism of interaction remains to be elucidated. As an approach to determining the disease-causing potential of a specific somatic mutation found in a person, iPSC technology provides advantages compared with ordinary methods, such as the use of transgenic cell lines. First,